

# Electrochemical regeneration of NaBH<sub>4</sub> from the hydrolysis reaction of NaBH<sub>4</sub> with the Ni-Co/Hydroxyapatite catalyst as a part of the hydrogen release cycle

Adrian Nur<sup>1\*</sup>, Arif Jumari<sup>1</sup>, Muhammad Dani Supardan<sup>2</sup>, Nazriati<sup>3</sup>, Zidan Insa Fauzi<sup>1</sup>, Reza Pratama Aditia<sup>1</sup>, Setiana Handayani<sup>1</sup>, and Arvian Raditya Airlangga<sup>1</sup>

<sup>1</sup>Departement of Chemical Engineering, Universitas Sebelas Maret, Surakarta, Indonesia

<sup>2</sup>Department of Chemical Engineering, Universitas Syiah Kuala, Banda Aceh, Indonesia

<sup>3</sup>Department of Chemistry, Faculty of Mathematics and Natural Sciences, Universitas Negeri Malang, Indonesia

**Abstract.** Sodium borohydride (NaBH<sub>4</sub>) is a high-hydrogen-content chemical hydride, but its practical use requires an efficient regeneration route from the hydrolysis by-product (NaBO<sub>2</sub>·2H<sub>2</sub>O). This work investigates a two-step NaBH<sub>4</sub>-H<sub>2</sub> cycle comprising catalytic hydrogen release and electrochemical regeneration of NaBH<sub>4</sub>. A Ni-Co/hydroxyapatite (HAp) catalyst was synthesized by an electrochemical one-step deposition route (160 mA cm<sup>-2</sup>, 90 min). The catalyst shows nano-sized primary particles (≈10–100 nm) agglomerated into 1–5 μm secondary clusters. The results of catalyst characterization with FTIR confirmed the presence of HAp with additional peaks indicating surface carbonaceous species. XRD of the catalyst identifies a composite of HAp with oxidized Ni/Co phases (NiCo<sub>2</sub>O<sub>4</sub> and CoO), evidencing successful incorporation of Ni-Co active phases on the HAp support. Mechanistically, the Ni/Co oxide surface is expected to provide hydrogen-activation (H\* formation) and borate adsorption sites, while HAp enhances dispersion and interfacial hydroxyl/phosphate functionality—together facilitating the hydrogenation of NaBO<sub>2</sub>·2H<sub>2</sub>O toward NaBH<sub>4</sub> when H<sub>2</sub> is supplied electrochemically. In this work, NaBH<sub>4</sub> was first hydrolyzed in water using an electrochemically synthesized Ni-Co/hydroxyapatite catalyst to release H<sub>2</sub> and form borate, and the spent solution was then regenerated electrochemically in a two-chamber cell separated by a bipolar membrane. In-situ hydrogen generated via cathodic water reduction was utilized to convert NaBO<sub>2</sub>·2H<sub>2</sub>O back to NaBH<sub>4</sub>. Regeneration was evaluated at current densities of 0.10–0.20 A cm<sup>-2</sup> for up to 120 min. NaBH<sub>4</sub> concentration increased with both electrolysis time and current density, reaching ~0.020 mol L<sup>-1</sup> at 0.20 A cm<sup>-2</sup> after 120 min (compared with ~0.017 mol L<sup>-1</sup> at 0.10 A cm<sup>-2</sup>). These results demonstrate the feasibility of coupling hydrogen release and electrochemical regeneration in a closed.

\* Corresponding author: [adriannur@staff.uns.ac.id](mailto:adriannur@staff.uns.ac.id)

## 1 Introduction

Hydrogen is widely regarded as a promising energy carrier for decarbonizing power generation and transport, yet its practical deployment is constrained by the need for safe, compact, and on-demand storage and release [1, 2]. One attractive route is chemical hydrogen storage [3, 4, 5, 6], where hydrogen is stored in stable compounds and released when needed. Among chemical hydrides, sodium borohydride ( $\text{NaBH}_4$ ) offers high theoretical hydrogen content and can generate hydrogen at mild conditions through hydrolysis; however, uncatalyzed hydrolysis is too slow to be practical, and the process produces sodium metaborate hydrate ( $\text{NaBO}_2 \cdot 2\text{H}_2\text{O}$ ) as a spent by-product that must be regenerated to close the cycle.

A large body of work has therefore focused on designing catalysts that accelerate  $\text{NaBH}_4$  hydrolysis while maintaining durability and low cost. The catalytic reaction mechanism of hydrolysis and methanolysis of  $\text{NaBH}_4$  occurs through the reaction of  $\text{BH}_4^-$  with the active site of the catalyst and the reaction of  $\text{OH}^-$  ions breaking the bond to form  $\text{H}_2$  [4, 6, 7, 8]. Ni- and Co-based catalysts are among the most studied non-noble options because they can provide high activity at substantially lower cost than Pt-, Ru-, or Pd-based systems.

In our previous study, we demonstrated that an electrochemically synthesized Ni-Co/hydroxyapatite (HAp) catalyst effectively promotes  $\text{NaBH}_4$  hydrolysis; significantly, catalyst formation parameters (current density and electrolysis time) strongly influenced performance, and the highest hydrogen generation rate was obtained at a catalyst-synthesis current density around  $92 \text{ mA cm}^{-2}$ . That work also reported apparent kinetic parameters (first-order behavior and Arrhenius-type dependence) that support the role of Ni-Co active sites in accelerating the hydrolysis pathway [8, 9].

Despite extensive studies, the physicochemical rationale for combining Ni and Co—especially when dispersed/impregnated on a functional support—should be clearly articulated, as it underpins catalyst selection. Co species are often reported to be intrinsically more active than Ni for borohydride hydrolysis, while Ni-Co bimetallic combinations can outperform either metal alone due to synergistic effects. For example, comparative studies on Ni vs Co systems indicate that Ni can exhibit lower apparent activity, partly attributed to strong surface hydrogen coverage that hinders reactant adsorption, whereas adding Co can increase the hydrogen generation rate. At the materials level, Ni and Co offer complementary characteristics: both metals can access multiple oxidation states and form catalytically active surface phases (e.g., oxides/oxyhydroxides, borides under borohydride environments), enabling (i)  $\text{BH}_4^-$  adsorption/activation, (ii) water activation to provide  $\text{OH}^-/\text{H}^*$  intermediates, and (iii) facile electron transfer at the metal/support interface. In Ni-Co systems, Co sites are frequently associated with efficient water activation, while Ni can help stabilize reactive hydrogen species; together, they can reduce kinetic barriers compared to monometallic catalysts, as also reflected in multiple reports on Ni-Co catalysts for  $\text{NaBH}_4$  hydrolysis [8, 9].

The role of the support is equally important. Hydroxyapatite ( $\text{Ca}_{10}(\text{PO}_4)_6(\text{OH})_2$ ) provides a chemically robust, ionically functional surface with phosphate and hydroxyl groups that can anchor Ni/Co species and enhance dispersion, increasing the accessible active area and improving stability against sintering and leaching. In the present work, the catalyst is a Ni-Co/HAp composite that (based on our characterization) contains HAp together with oxidized Ni/Co phases (e.g.,  $\text{NiCo}_2\text{O}_4$  and  $\text{CoO}$ ), indicating successful incorporation of Ni-Co active phases on the HAp framework [8, 9, 10].

Such supported, highly dispersed bimetallic systems are expected to provide abundant interfacial sites where borohydride species and water-derived intermediates can react efficiently—consistent with the previously observed catalytic function of Ni-Co/HAp.

However, hydrogen release alone does not ensure a viable storage technology. The critical bottleneck for  $\text{NaBH}_4$ -based hydration of  $\text{NaBH}_4$  from  $\text{NaBO}_2 \cdot 2\text{H}_2\text{O}$ . Many regeneration approaches reported in the literature are chemically intensive, require external reducing agents, or demand complex processing steps, thereby increasing costs and undermining sustainability. By contrast, electrochemical regeneration offers a pathway to integrate regeneration with renewable electricity, but reported configurations often still rely on externally supplied hydrogen or conditions that are difficult to integrate directly with a practical “hydrogen release–regeneration” loop. The key opportunity is therefore to design a process that (i) couples hydrolysis and regeneration, and (ii) uses readily available, controllable hydrogen equivalents generated electrochemically.

The novelty of this study, in comparative terms, is that we integrate (1) catalytic  $\text{NaBH}_4$  hydrolysis using an electrochemically prepared Ni–Co/HAp catalyst with (2) electrochemical regeneration of  $\text{NaBH}_4$  from the same spent hydrolysis solution in a two-chamber cell separated by a bipolar membrane, where the reductant is in-situ hydrogen generated by cathodic water reduction rather than externally supplied hydrogen.

This configuration directly targets the principal gap between “high hydrolysis activity” studies and “stand-alone regeneration” studies, aiming to move closer to a closed  $\text{NaBH}_4$ – $\text{H}_2$  cycle. In this work, regeneration performance is systematically evaluated as a function of current density ( $0.10$ – $0.20 \text{ A cm}^{-2}$ ) and electrolysis time (up to 120 min), enabling a quantitative assessment of how the electrical driving force controls  $\text{NaBH}_4$  recovery.

Accordingly, this paper (i) synthesizes Ni–Co/HAp via an oute, (ii) characterizes the resulting catalyst structure and phases, (iii) evaluates  $\text{NaBH}_4$  hydrolysis behavior in water using the prepared catalyst, and (iv) demonstrates electrochemical regeneration of  $\text{NaBH}_4$  from  $\text{NaBO}_2 \cdot 2\text{H}_2\text{O}$  in a bipolar-membrane reactor using in-situ cathodic hydrogen. The combined approach is intended to provide an experimentally grounded, quantitatively evaluated basis for advancing  $\text{NaBH}_4$  toward a more practical, regenerative.

## 2 Experimental

### 2.1 The synthesis and Characterization of the catalyst

The catalyst used in this research is Ni-Co, supported on hydroxyapatite. The catalyst synthesis method is electrochemical, as described in our previous research [9, 10]. The catalyst synthesis, as in our previous work, used  $\text{NiCl}_2$ ,  $\text{CoCl}_2$ ,  $\text{CaCl}_2$ ,  $\text{KH}_2\text{PO}_4$ , Na-EDTA, NaOH, and HCl, all from MERCK. XRD (Shimadzu 6000 X-ray), SEM (S40 Survey FEI), and FTIR (Shimadzu Ir-Spirit FTIR) were used to characterize the Ni-Co/hydroxyapatite catalyst obtained. The electrolyte course of action composition is  $0.1\text{M NiCl}_2$ ,  $0.1\text{M CoCl}_2$ ,  $0.1\text{M NaBH}_4$ ,  $0.25\text{M CaCl}_2$ ,  $0.15\text{M KH}_2\text{PO}_4$ , and  $0.25\text{M Na}_2\text{H}_2\text{EDTA} \cdot 2\text{H}_2\text{O}$ . The anode and cathode electrodes (from carbon) were  $5 \times 2 \times 0.4 \text{ cm}$ . The bipolar membrane is from Fumatech BWT GmbH. The electrodes were related to a control supply. The current density utilized was  $160 \text{ mA/cm}^2$ . Electrolysis was carried out at 90 minutes. XRD examination was carried out using a Shimadzu 6000 X-ray diffractometer (XRD) with  $\text{CuK}\alpha$  ( $\lambda = 1.5406 \text{ nm}$ ) radiation with a step of  $0.7^\circ \cdot \text{s}^{-1}$  over exact ranges ( $2\theta$ ) from  $20$  to  $60^\circ$ . SEM examination was satisfied by the S40 Survey FEI using a speeding-up voltage of  $20 \text{ kV}$ .

### 2.2 Hydrolysis of $\text{NaBH}_4$ to release hydrogen

The hydrolysis reaction was carried out by adding  $0.567 \text{ g}$  of  $\text{NaBH}_4$  and  $0.08 \text{ g}$  of catalyst to  $150 \text{ mL}$  of water in a closed Erlenmeyer flask placed in a water bath (Fig 1.). When the

reaction takes place, hydrogen is released.  $\text{NaBH}_4$  concentration was analyzed using the Iodate method [24] by taking 5 mL samples every 15 minutes.

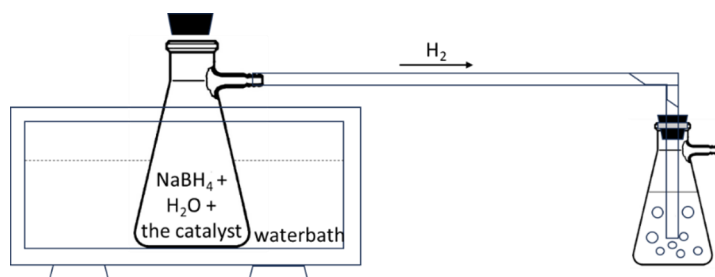


**Fig. 1.**  $\text{NaBH}_4$  hydrolysis experimental tool to release hydrogen

### 2.3 $\text{NaBH}_4$ Regeneration

$\text{NaBH}_4$  regeneration was performed in a two-chamber electrochemical cell (Fig. 2) using the remaining  $\text{NaBH}_4$  solution resulting from the  $\text{NaBH}_4$  hydrolysis experiment. An electrochemical cell consists of 2 chambers (an anode chamber and a cathode chamber), separated by a bipolar membrane. The two electrodes used are carbon electrodes connected to a power supply. The current densities used were 0.1, 0.15, and 0.2  $\text{A}/\text{cm}^2$ , with an electrolysis time of 120 minutes.  $\text{NaBH}_4$  concentration was tested using the Iodate titration method. This method is based on the reaction of  $\text{NaBH}_4$  with  $\text{KIO}_3$ , followed by back-titration of the excess iodate with the  $\text{I}/\text{I}_2\text{-S}_2\text{O}_3^{2-}$  system.

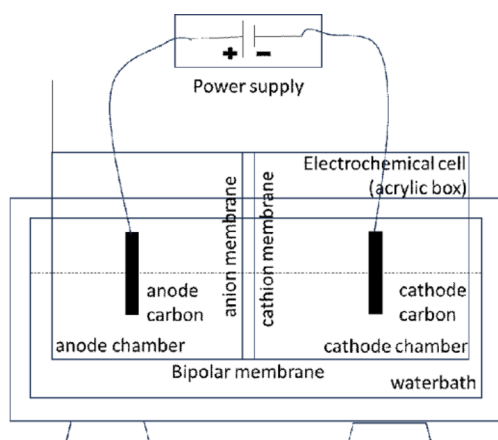


**Fig. 2.**  $\text{NaBH}_4$  regeneration experiment tools

## 3 Results & Discussion

### 3.1 Characterization of the catalysts

Scanning Electron Microscopy analyzes the surface morphology of the catalyst. The morphology of the catalyst particles is shown in Figure 3. This fig cannot distinguish Ni, Co, and hydroxyapatite particles. The catalyst appears as small, nano-sized spherical particles

that form larger, irregularly shaped particles. The diameter of primary particles is between 10 - 100 nm (Figure 3). Primary particles agglomerate into secondary particles with a 1 - 5  $\mu\text{m}$  diameter [11].

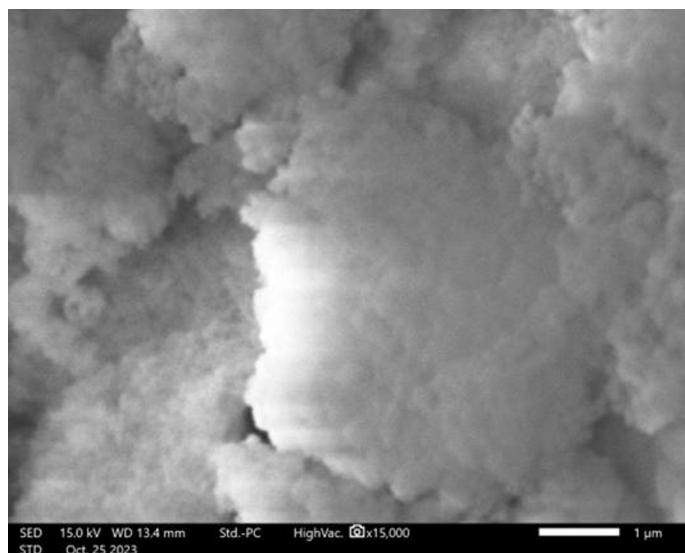


**Fig. 3.** The particle morphology of the Ni-Co/hydroxyapatite catalyst with a magnification of 15,000

Figure 4 shows the functional groups of catalyst particles analyzed by FTIR [12]. The presence of peaks at wave numbers  $3300\text{ cm}^{-1}$  and  $1000 - 500\text{ cm}^{-1}$  indicates the presence of  $\text{OH}^-$  and  $\text{PO}_4^{3-}$  functional groups, which are hydroxyapatite functional groups. At wave numbers of  $2000\text{ cm}^{-1}$  and  $1630\text{ cm}^{-1}$ , peaks are visible, indicating the presence of C-H and C=C groups, which suggests the formation of carbon compounds on the catalyst.

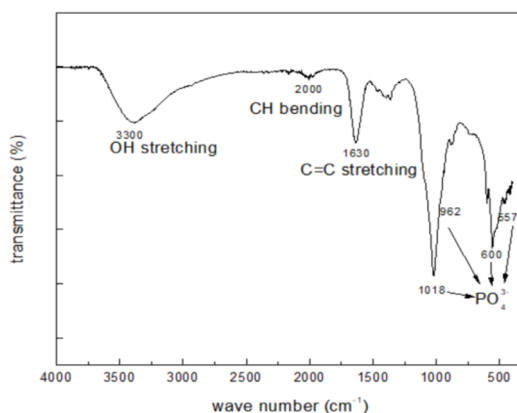


**Fig. 4.** FTIR analysis of Ni-Co/hydroxyapatite catalyst

The XRD phase identification results (Figure 5) show that the peaks match  $\text{NiCo}_2\text{O}_4$ ,  $\text{CoO}$ , and hydroxyapatite particles. Ni-Co/hydroxyapatite catalyst has been successfully synthesized. A composite of hydroxyapatite and an oxidized Ni and Co catalyst— $\text{NiCo}_2\text{O}_4$  and  $\text{CoO}$ —make up the particles. Hydroxyapatite is demonstrated by the presence of peaks  $26^\circ$  and  $32^\circ$  [13]. Particles of  $\text{NiCo}_2\text{O}_4$  are mentioned in peaks  $31^\circ$  and  $36^\circ$  [14].  $\text{CoO}$  particles are shown by the presence of a peak at  $34^\circ$ . XRD confirms that the composite contains hydroxyapatite together with additional reflections consistent with  $\text{CoO}$  and spinel  $\text{NiCo}_2\text{O}_4$

by comparison with reference patterns. The oxide-related reflections are absent in pristine HAp and appear only after Ni–Co deposition. XRD demonstrates phase presence but not spatial distribution.

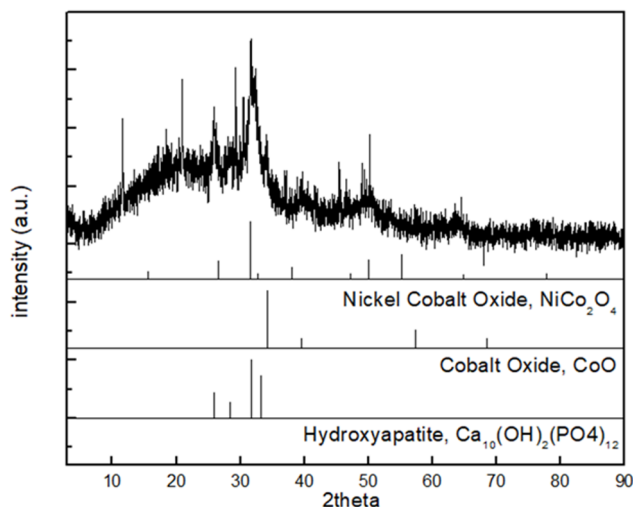
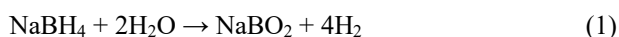


**Fig. 5.** X-ray Diffractogram of Ni-Co/hydroxyapatite catalyst

### 3.2 The Hydrolysis of NaBH<sub>4</sub> to release hydrogen and the regeneration of NaBH<sub>4</sub>

Figure 6 shows the concentration of NaBH<sub>4</sub> in the hydrolysis process. The concentration of NaBH<sub>4</sub> decreased with increasing hydrolysis time. During the hydrolysis process, NaBH<sub>4</sub> releases hydrogen, forming NaBO<sub>2</sub>. The reaction of NaBH<sub>4</sub> with water has occurred according to the following reaction equation:



As a result, the concentration of NaBH<sub>4</sub> decreased with increasing time. Factors influencing the kinetics of hydrogen release from NaBH<sub>4</sub> include pH, temperature, solution concentration, catalyst size, and stirring [15]. The hydrolysis of borohydride is strongly pH-dependent because BH<sub>4</sub><sup>-</sup> is more stable in alkaline media, while hydrolysis accelerates as the medium becomes less alkaline. In addition, pH influences catalyst surface chemistry (hydroxylation/charge) and the availability of reactive water-derived intermediates. Temperature increases the hydrolysis rate by lowering the effective kinetic barrier. Increasing initial NaBH<sub>4</sub> concentration increases the theoretical hydrogen capacity but can alter observed kinetics due to changes in ionic strength, viscosity, and accumulation of borate products, which may inhibit active sites or shift local pH. Smaller catalyst particles typically provide higher accessible surface area and shorter diffusion lengths, increasing the number of exposed Ni–Co active sites per unit mass. Stirring controls external mass transfer of BH<sub>4</sub><sup>-</sup> to catalytic sites and removal of hydrogen bubbles from the catalyst surface. At low stirring, bubble coverage and boundary-layer limitations can suppress apparent kinetics; increasing stirring typically raises the observed rate until a plateau is reached where the process becomes reaction-controlled.

As reaction (1) progresses, BH<sub>4</sub><sup>-</sup> ions are converted to borate species (NaBO<sub>2</sub>/borate hydrates), so the measured NaBH<sub>4</sub> concentration must decline. The nearly linear decrease in Fig. 6 suggests that, under the tested conditions, the system operates close to an approximately constant rate regime over 15–90 min (often observed when catalyst surface

sites are abundant and the surface reaction controls the overall rate). As  $\text{NaBH}_4$  becomes lower, the rate can eventually slow due to reduced  $\text{BH}_4^-$  availability and/or changes in solution chemistry (e.g., pH shift, borate accumulation), which can inhibit further hydrolysis. The Ni–Co/HAp catalyst accelerates  $\text{NaBH}_4$  hydrolysis mainly by providing active surface sites that lower the activation barrier for the elementary steps:

- $\text{BH}_4^-$  adsorption/activation on Ni/Co sites: Ni and Co surfaces can facilitate B–H bond activation, forming reactive surface hydrogen intermediates ( $\text{H}^*$ ) and boron-containing surface species.
- Water activation: Co/Ni sites can also promote water dissociation, supplying  $-\text{OH}$  species needed to form borate while simultaneously enabling  $\text{H}^*$  formation and  $\text{H}_2$  recombination.
- Synergy of Ni–Co: Bimetallic Ni–Co systems often show higher activity than monometallic ones because Ni and Co can contribute complementary functions (e.g., water activation vs hydrogen recombination), increasing the overall turnover.
- Role of HAp support: Hydroxyapatite helps disperse Ni/Co phases (more exposed active area) and provides a surface rich in  $-\text{OH}/\text{PO}_4^{3-}$  functionalities, improving anchoring and stabilizing the catalytic phase against agglomeration/leaching.

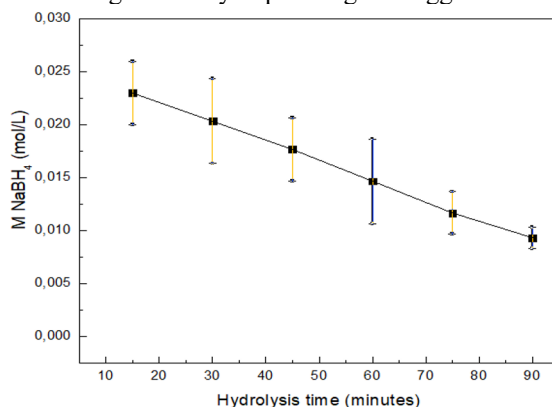


Fig. 6.  $\text{NaBH}_4$  concentration during hydrolysis time

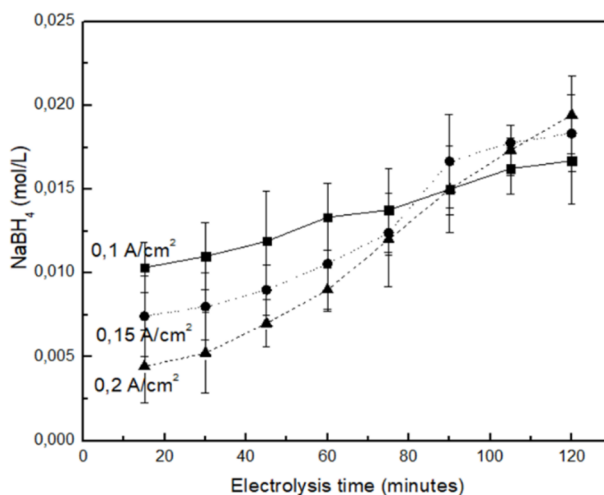


Fig. 7.  $\text{NaBH}_4$  concentration during electrolysis time at various current densities

The concentration of  $\text{NaBH}_4$  during the electrolysis process for regeneration of  $\text{NaBH}_4$  at various current densities is shown in Figure 7. In general, the concentration of  $\text{NaBH}_4$  increases with increasing electrolysis time. The increase in  $\text{NaBH}_4$  concentration occurs due to the reaction of  $\text{NaBO}_2$  with hydrogen obtained from the reduction of water, which forms  $\text{NaBH}_4$  so that the concentration of  $\text{NaBH}_4$  increases. The effect of current density shows that the greater the current density, the faster the increase in  $\text{NaBH}_4$  concentration. The  $\text{NaBH}_4$  concentration increases slowly at early times and then rises more steeply around ~70–90 min, especially at 0.15 and 0.20  $\text{A cm}^{-2}$  (the curves start to climb faster and begin to separate more clearly). This is the point where the regeneration rate becomes visibly higher than in the first ~0–60 min.

A standard electrochemical explanation is a transition from an initial “conditioning/low-effective rate” period to a regime where more reducing equivalents become available and are used more efficiently. In the early stage (0–60 min), part of the applied current can be consumed by:

- electrode activation and surface conditioning (wetting, removal/formation of oxide layers, establishment of steady surface state),
- build-up of local pH gradients and stabilization of ion transport through the bipolar membrane,
- mass-transfer limitations while reactants/products accumulate and reach a quasi-steady concentration boundary layer.

Once the cell reaches a more stable electrochemical environment, hydrogen generation (as reducing equivalents) becomes more continuous, and the reaction between borate species and hydrogen (or hydrogen-derived intermediates) proceeds faster—hence the more pronounced increase in  $\text{NaBH}_4$  after ~70–90 min.

The greater the current density, the faster the addition of hydrogen, and the greater the reaction of hydrogen with  $\text{NaBO}_2$  to form  $\text{NaBH}_4$ . At a fixed electrode area, the hydrogen production rate increases with current density, because hydrogen formation at the cathode is proportional to current (Faraday’s law). So, for the same electrolysis time  $t$ , the moles of  $\text{H}_2$  produced follow:  $0.20 \text{ A cm}^{-2} > 0.15 \text{ A cm}^{-2} > 0.10 \text{ A cm}^{-2}$ . This matches Figure 7, the 0.20  $\text{A cm}^{-2}$  curve shows the fastest rise in  $\text{NaBH}_4$  concentration, consistent with the highest hydrogen (reducing equivalents) generation per unit time. The quantity of regenerated  $\text{NaBH}_4$  is still tiny, so the right conditions are needed for the electrochemical regeneration of  $\text{NaBH}_4$ .

## 4 Conclusions

The catalyst used in this paper is Ni-Co/hydroxyapatite, which is used in the  $\text{NaBH}_4$  hydrolysis reaction to release hydrogen. The electrolysis reaction for the regeneration of  $\text{NaBH}_4$  was successfully carried out. The longer the electrolysis time, the higher the concentration of  $\text{NaBH}_4$ . The higher the current density, the higher the concentration of  $\text{NaBH}_4$ . The quantity of regenerated  $\text{NaBH}_4$  is still tiny, so the right conditions are needed for electrochemical regeneration of  $\text{NaBH}_4$ .

## 5 References

1. Usman MR. *Renew Sustain Energy Rev* 2022; **167**: 112743.
2. Amirthan T, Perera MSA. *J Nat Gas Sci Eng* 2022; **108**: 104843.
3. Yao J, Wu Z, Wang H, Yang F, Ren J, Zang Z. *J Energy Chem* 2022; **74**: 218-38.
4. Xu D, Zhang Y, Guo Q. *Int J Hydrogen Energy* 2022; **47**: 5929 – 46.
5. Wang T, Jiang T, Zhang H, Zhao Y. *Int J Hydrogen Energy* 2022; **47**: 14589 – 610.

6. Abdelhamid HN. *Int J Hydrogen Energy* 2021; **46**: 726 – 65.
7. Saka C. *Appl. Catal. B* 2021; **292**: 120165.
8. Nur A, Budiman AW, Jumari A, Karsten JM, Dewai PH, Asyabaniyah SL, Vashadinata Urganani J, Torres, FJ, Palumbo M, Baricco M. *Int J Hydrogen Energy* 2008; **33**: 3111 – 5.
9. Nur A, Budiman A. W., Jumari A., Nazriati N, Fajaroh F. *Chem Chem. Technol* 2021, **15**, 3, 389-394.
10. Nur A, Jumari A, Dyartanti ER, Paramitha T, Irianto RS, Ismarlina H, Prahaspati K, Kurniawan LA. *Evergreen* 2022; **9**: 421 – 6.
11. Al-Hamdan R.S., Al-Mutairi B., Kattan H.F., Alsuwailem N.A., Farooq I., Vohra F., Abduljabbar T., *Polymers* 2020; **12**: 2948
12. Abifarin JK, Obada DO, Dauda ET, Dodoo-Arhin D, *Data in brief* 2019; **26**: 104485
13. Peng H, Wang J, Lv S, Wen J, Chen JF. *Ceram Int* 2015; **41**: 14340 – 9.
14. Lee HJ, Park DH, Lee WJ, Han SB, Kim MH, Byeon JH, Park KW. *Appl. Catal., A* 2021; **626**: 118377.
15. Chen J, Wu Z, Zheng J, Shi Y, Xie L, Yang F, Wang Y, Zhang Z. *Chem Eng J* 2024; **486**: 150062.